Journal of MATERIALS RESEARCH

Article
DOI:10.1557/s43578-023-01182-8

Macrophage plasticity and differentiation on the decellularized human cornea

Juhi Chakraborty[1], Subhadeep Roy[1], Pranav Pandey[2], Sujata Mohanty[3], Radhika Tandon[2], Sourabh Ghosh[1,a)]

[1] Regenerative Engineering Laboratory, Department of Textile and Fibre Engineering, Indian Institute of Technology Delhi, Hauz Khas, New Delhi 110016, India
[2] Dr. Rajendra Prasad Centre for Ophthalmic Sciences, All India Institute of Medical Sciences, Ansari Nagar, New Delhi 110029, India
[3] Stem Cell Facility (DBT-Center of Excellence for Stem Cell Research), All India Institute of Medical Sciences, Ansari Nagar, New Delhi 110029, India
[a)] Address all correspondence to this author. e-mail: sourabh.ghosh@textile.iitd.ac.in

Sourabh Ghosh was an editor of this journal during the review and decision stage. For the JMR policy on review and publication of manuscripts authored by editors, please refer to http://www.mrs.org/editor-manuscripts/.

Received: 18 August 2023; accepted: 27 September 2023; published online: 5 October 2023

Several donated human corneas become unsuitable for transplantation due to lack of cellularity, diseases, and inadequate death to enucleation/preservation time. Here, we utilized discarded human corneas unsuitable for transplantation. Corneas were decellularized using a perfusion bioreactor with Triton-X 100 and cross-linked with chondroitin sulfate to reduce immune response, which FTIR and AFM confirmed. An in vitro study established the morphology of THP-1 cells cultured under three conditions, i.e., native, decellularized, and cross-linked for 10 days, by SEM analysis. The oxidative mechanism in THP-1 cells was determined by nitric oxide and reactive oxygen species in the media during the culture period. Cell surface markers and receptors were examined using RT-PCR. A panel of 40 identified cytokines/chemokines and release factors responsible for the immune response and implant rejection were estimated using cytokine microarray. Our findings elucidated the fundamentals of corneal rejection and helped identify a suitable decellularized matrix with predictive immunological properties.

Introduction

Strategies for regenerating full-thickness corneas with corneal epithelium and endothelium have been a subject of interest in ophthalmological research because of the limited availability of high-quality cadaveric donor tissues. Human corneal transplantation (HCT) is one of the most commonly performed procedures worldwide. The human cornea actively maintains its development and steady-state function without a blood supply or lymphatic system (corneal angiogenic privilege) [1]. The human cornea is an immune-privileged region of the body, so a nominal immune reaction is expected at such sites. Records of immune rejection in interpenetrating keratoplasty (25%) still exist because of the lack of understanding of MHC class II expression and macrophage/T helper cell interactions [2, 3]. Upregulation of pro-angiogenic signals elevates corneal neovascularization in the limbal region. Resident macrophages are crucial for maintaining the balance between injured and regenerating corneas [4]. They communicate with circulating monocytes to regulate inflammation and regeneration. Studies have shown that resident and bone marrow-derived macrophages exhibit extraordinary phenotypic plasticity, which dynamically orchestrates corneal infection and inflammation [5, 6]. Cell-guided tissue engineering strategies can be used to identify the immunogenic potential during corneal transplantation to avoid immune rejection.

Decellularization is one of the most promising techniques for organ and tissue regeneration. All cellular components (nuclear and cytosolic), debris, and antigens are removed from the extracellular matrix (ECM) during this process [7, 8]. Our group has previously demonstrated the potential of decellularization using a standardized perfusion bioreactor-based decellularization process [8]. Various research groups have attempted to use ionic/non-ionic detergent-mediated, acid/base-based

[9–11], enzymatic digestion [12, 13], and physical and miscellaneous methods for effective decellularization [14, 15]. Decellularized corneas may elicit an immune response after transplantation despite removing antigens and cellular constituents. One reason is that a hidden antigenic motif may be exposed during decellularization to identify the intermediate correlation between the upregulated and downregulated genes, which may cause a severe immunogenic response [16, 17]. However, immunological assessments have been poorly explained [18, 19]. Resident innate immune cells (CD11b+ macrophages), CD64+CCR2− macrophages, and circulating monocytes have been largely neglected in previous studies [20, 21]. Moreover, the mechanism by which circulating monocytes receive cytokine signals from host-resident macrophages in response to decellularized tissue after implantation remains unknown [22, 23]. The heterogeneity and versatility of macrophages in a particular tissue are due to their dynamic shift from bone marrow progenitor cells [24]. In this respect, in our previous study [16], we implanted three corneal scaffolds obtained from native, decellularized, and decellularized corneas conjugated with oxidized chondroitin sulfate (CS) into rabbit stroma. Three months after implantation into the rabbit corneal stromal region, histological analysis confirmed restoration of the collagen fibril conformation and migration of cells to the implanted constructs, confirming proper graft integration. Our study involving healthy monocytes and differentiated macrophages with their surface marker analysis using the intracellular pH indicator pHrodo red, acidic organelle tracker Lysotracker red, ER tracker, and exosome markers CD63 and LAMP-2 antibodies confirmed that cross-linked decellularized matrices elicited the most negligible immune response compared to decellularized matrices [16]. It is important to note that

CS used for the conjugation of decellularized corneas plays a key role wound healing [25], apart from abating immune response [26] and improving mechanical strength [27]. However, we investigated the immunogenic potential of decellularized and cross-linked goat corneas across species (goat to rabbit). Before proceeding to a human clinical trial, we must validate whether decellularization of the human stromal layer using discarded human corneas unsuitable for implantation can trigger an immune response.

Several researchers have attempted to develop 3D bioengineered human Cornea. However, they failed to replicate the parallel collagen fibril orientation present in the native cornea. Amniotic membrane transplantation has several disadvantages, including bacterial, fungal, or viral infections and premature degradation. Residual subepithelial membranes in the amniotic membrane sometimes increase the opacity of the visual axis [28]. Researchers have also tried to develop an electrospun nanofiber scaffold for corneal implantation; however, solvents used in electrospun nanofibers are often acidic, which may affect cytocompatibility and immune response [29, 30].

This study validated our previously established hypothesis [16] by using residual human donor corneal remnants after transplantation. Specifically, we have focused on the following aspects:

a. The first objective was to determine whether cross-linking decellularized corneas with CS helps to change the plasticity of healthy monocytes into M2 macrophages to reduce graft rejection. Cytokine microarray and genomic data analyses were used to identify cytokine profiles and to predict differential plasticity (M1 and M2).
b. Second, we elaborated that the role of monocytes/macrophages as infiltrating cells is crucial for graft rejection. Our study also explains corneal rejection after penetration/Ant. Lamellar keratoplasty is possibly due to macrophage-mediated and lymph angiogenesis.
c. Third, the specific plasticity of resident tissue macrophages in the human cornea under both healthy and pathological conditions remains unknown.

To the best of our knowledge, this is the first study to use healthy monocytes cultured on decellularized or chemically modified discarded human corneal surfaces to predict transplant immunology and in vivo reprogramming. Our previous study has highlighted the role of CS in cartilaginous disk tissue regeneration [31]. Here, we observed that the CS-cross-linked discarded decellularized corneal matrix changed the plasticity of healthy monocytes toward an anti-inflammatory M2 phenotype. In contrast, the normal decellularized matrix supported the pro-inflammatory M1 phenotype. In vitro approaches will help to identify ideal discarded corneal substitutes for transplantation with predictive immunological profiles and in vivo reprogramming. This would serve as an excellent alternative to current animal models. This strategy opens up a new possibility to investigate the possible immune responses. We would now employ discarded human corneas for anterior lamellar keratoplasty in patients by following the same principles of decellularization and chemical cross-linking.

Results

Cross-linked cornea ultrastructure analysis

The decellularized cornea (DC) was characterized by residual GAG and DNA content (Supplementary Table 7) and the absence of cell nuclei. Deconvolution was performed from 900 to 1800 cm^{-1}. The peak at 1610–1620 cm^{-1} representing the collagen I component, was absent in FTIR analysis. The amide I peak shift from 1634 to 1628 cm^{-1} was due to the interaction

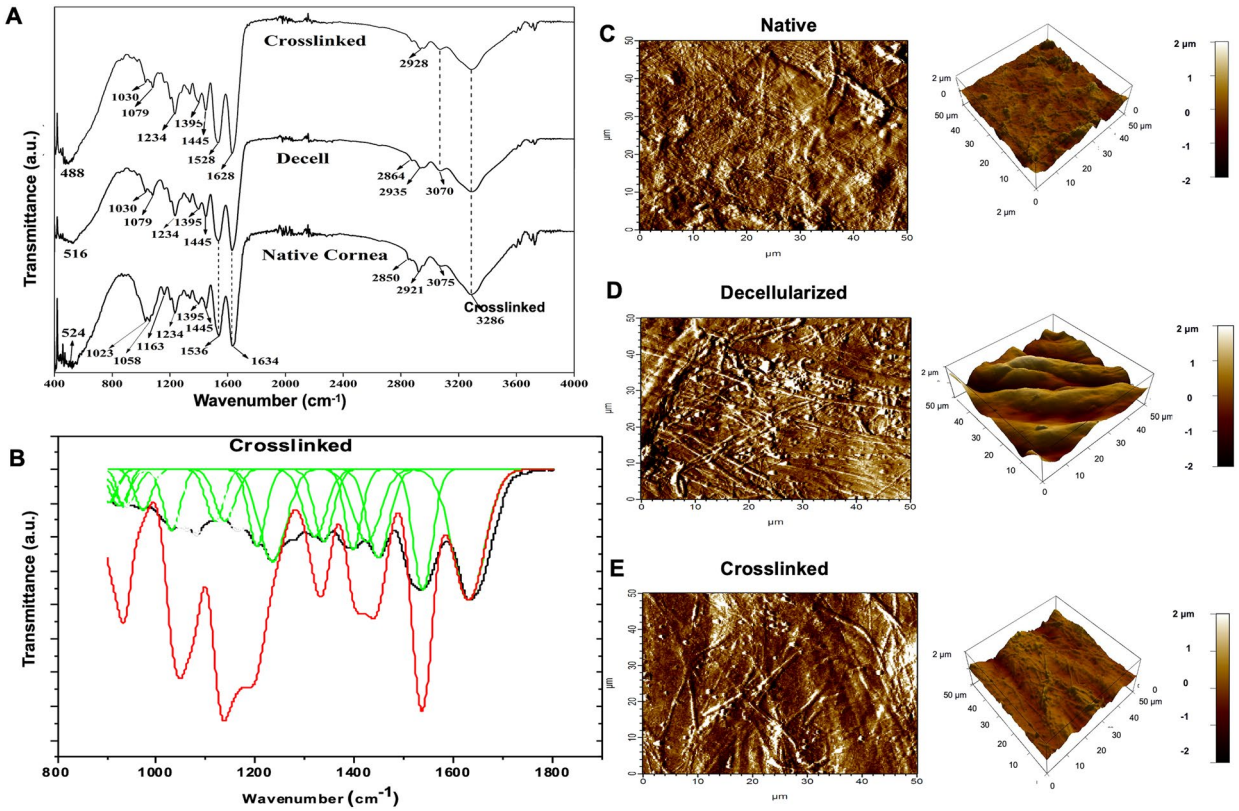

Figure 1: Physical characterization of native, decellularized, and cross-linked human corneas. (A) FTIR plots of native, decellularized, and cross-linked chondroitin sulfate. 240 infrared spectrum scans were taken in transmittance mode in the spectral region of 400–4000 cm^{-1} with a spectral resolution of 4 cm^{-1} for each sample. The peaks in the spectral area were obtained using Origin 8.5. (B) Deconvoluted peaks of chondroitin sulfate-cross-linked human corneas from 900 to 1800 cm^{-1}. AFM images of native (C), decellularized (D), and chondroitin sulfate cross-linked (E) corneas. Micrographs were captured using a Tap300Al cantilever with a spring constant of 40 N/m and a resonance frequency of 300 kHz at a scanning rate of 0.5 at different scanning areas.

between the COO^- and SO_3^- of CS and the C=O of collagen. Redshifts denote these phenomena, as shown in the figure [Fig. 1(B)]. COO^- and SO_3^- ions in CS were observed at 1628 and 1238 cm^{-1}, respectively. No changes were observed at 1234 cm^{-1}, which were assigned to amide III vibrations of the corneal epithelial collagen type I layer. The peak at 1350 cm^{-1} is assigned to the symmetric methyl bending vibrations of the acetate anion of CS Amide II, positioned at 1536 cm^{-1}, corresponding to N–H and C–H stretching vibrations and C–O stretching vibrations, respectively. Nominal changes were observed at 1536–1528 cm^{-1} for the cross-linked samples [Fig. 1(A) and (B); Supplementary Table 3].

Atomic force microscopy was performed to understand high-resolution nanoscale surface topological changes. The native cornea (NC) had a lower surface roughness (232.7 ± 0.001 nm) than the DC (266.7 ± 0.002 nm) samples. The DC showed extensive collagen fibril orientation due to the removal of the ECM. The CS-cross-linked human cornea exhibited lower surface roughness (248.8 ± 0.001 nm) than the DC [Fig. 1(C), (D), and (E); Supplementary Table 6].

Morphological analysis of adhesion activation

Figures 2 and 3 illustrate distinct morphological characteristics among the different groups. THP-1 monocytes cultured on DC and NC were analyzed to identify their morphologies on different corneal surfaces. The cells on the NC were predominantly round and had a larger cell surface area than the M0 macrophages, whereas that on the DC exhibited pancake like morphology. The cells on the CS-cross-linked matrix often exhibited elongated and spread morphology. THP-1 cells grown on decellularized, and native surfaces appeared to penetrate the matrix after 10 days of culture. The surface of the matrix was visibly degraded, with a large distribution of pores. Cells tended to maintain smaller footprints with flattened patterns on decellularized and native corneal surfaces, whereas CS-cross-linked surface cells exhibited highly spread and elongated morphology with greater filopodia (Figs. 2 and 3).

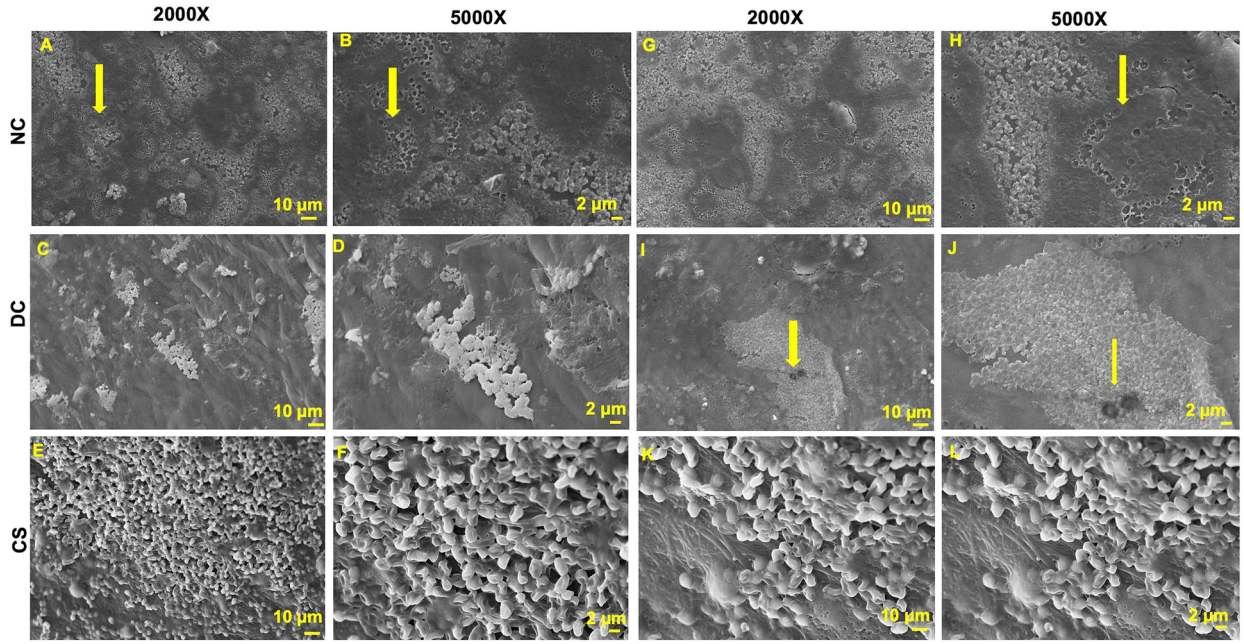

Figure 2: SEM images of THP-1 cells cultured on different patient corneal scaffolds for 10 days. Patient Sample—OEB1043. NC (A, B), DC (C, D), CS (E, F). Patient Sample—16042A. NC (G, H), DC (I, J), CS (K, L). The yellow arrow indicates (A, G) surface degradation (J). All the samples were imaged using a JEOL 5610 LV instrument at an accelerating voltage of 5 kV. The samples were imaged at two different magnifications, respectively, × 2000 and × 5000, with scale bars of 10–2 µm; where *NC* native cornea, *DC* decellularized cornea, *CS* CS cross-linked decellularized cornea.

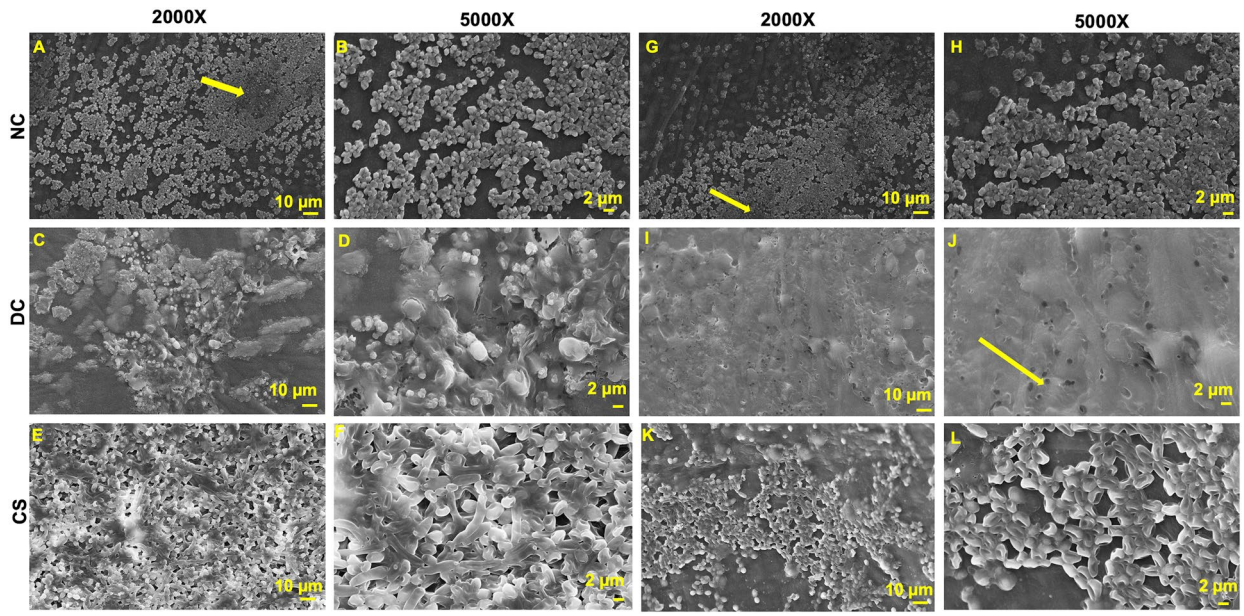

Figure 3: SEM images of THP-1 cells cultured on different patient corneal scaffolds for 10 days. Patient Sample—16038B. NC (A, B), DC (C, D), CS (E, F). Patient Sample—16036A. NC (G, H), DC (I, J), CS (K, L). The yellow arrow indicates (I, J) surface degradation (A, B, H). All the samples were imaged using a JEOL 5610 LV instrument at an accelerating voltage of 5 kV. The samples were imaged at two different magnifications, respectively, × 2000 and × 5000, with scale bars of 10–2 µm; where *NC* native cornea, *DC* decellularized cornea, *CS* CS cross-linked decellularized cornea.

Biochemical analysis

The metabolic activity of THP-1 cells cultured on different corneal surfaces (NC, DC, CS-cross-linked) was analyzed for the NO and ROS release patterns. The ROS release pattern of monocytes in control and cross-linked corneas was much lower [4-fold ($p < 0.0001$)] than that in DC, as indicated by the DPPH-dependent assay. Monocytes cultured on cross-linked

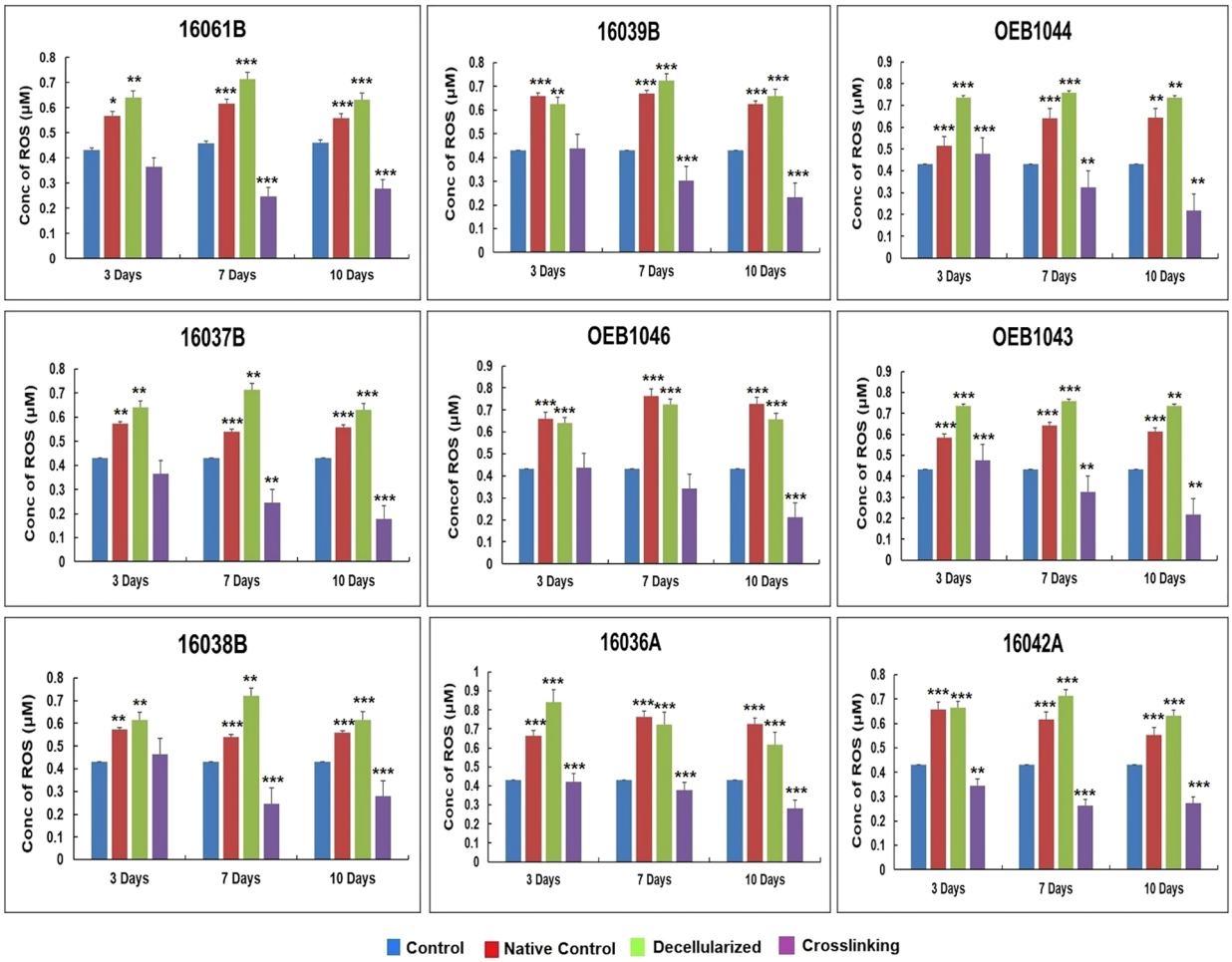

Figure 4: Release assay for reactive oxygen species in 16061B (A), 16039B (B), OEB1044 (C), 16037B (D), OEB1043 (E), OEB1046 (F), 16038B (G), 16036A (H), 16042A (I) nine patient sample at days 3, 7 and 10. GraphPad Prism 6 was used to perform one-way ANOVA. All data are presented as mean ± SD, statistical significance ($p < 0.05$). Each experiment was performed in triplicates and repeated twice.

corneas (OEB 1043) showed a higher ROS release pattern on day 3 (425 μM), which subsided on days 7 (228 μM) and 10 (176 μM). A similar ROS release pattern was observed in the remaining cross-linked samples. Monocytes grown on the DC (16061 B, 16037 B, 16038 B, 16,039 B) exhibited maximum ROS release (768 μM) on day 3 and maintained their levels on days 7 and 10 (Fig. 4; Supplementary Table 4).

The decellularized and native corneas showed a higher NO release [1.75-fold ($p < 0.0001$)] pattern than the control on day 3 for the 16061 B patient sample. Cross-linked corneas exhibited a much lower NO release pattern [1.5-fold ($p < 0.0001$)] than DC and NC. The remaining seven patient samples (OEB1044, 16037B, OEB1043, OEB1046, 16038 B, 16036A, and 16042A) showed a similar NO release pattern in the DC. Higher NO release was observed after 3, 7, and 10 days. In comparison, the cross-linked cornea showed higher NO release at 3 days but subsided at 7- and 10-days (Fig. 5; Supplementary Table 5).

Gene expression analysis

A panel of pro-inflammatory (M1-MMP2, MMP13, VEGF, and IL6R1) and anti-inflammatory (M2-CXCR1 and MMP1) genes was screened to identify the polarization of monocytes on NC, DC, and CS-cross-linked corneal surfaces at 10 days. CXCR1 expression was highest [6 ± 0.02-fold ($p < 0.05$)] in monocytes cultured on NC and DC patient samples (6 ± 0.02-fold, $p < 0.05$). The remaining patient samples (16037 B, 16061 B, OEB1044, OEB1046, 16038B) exhibited a similar pattern of CXCR1 expression in NC and DC patient samples and showed up to [3.5 ± 0.02-fold ($p < 0.05$)] higher expression. MMP1 expression in monocytes on the NC and DC patient surfaces was the highest [4 ± 0.02-fold ($p < 0.05$)] in the samples of five patients (16036A, 16061 B, OEB1044, OEB1046, 16038B).

In contrast, monocytes cultured on CS-cross-linked corneal surfaces showed the lowest expression of MMP2 and VEGF among all patient samples (16037 B, 16061 B, OEB1044, OEB1046, 16038 B, 16039 B, OEB1043, 16036A,

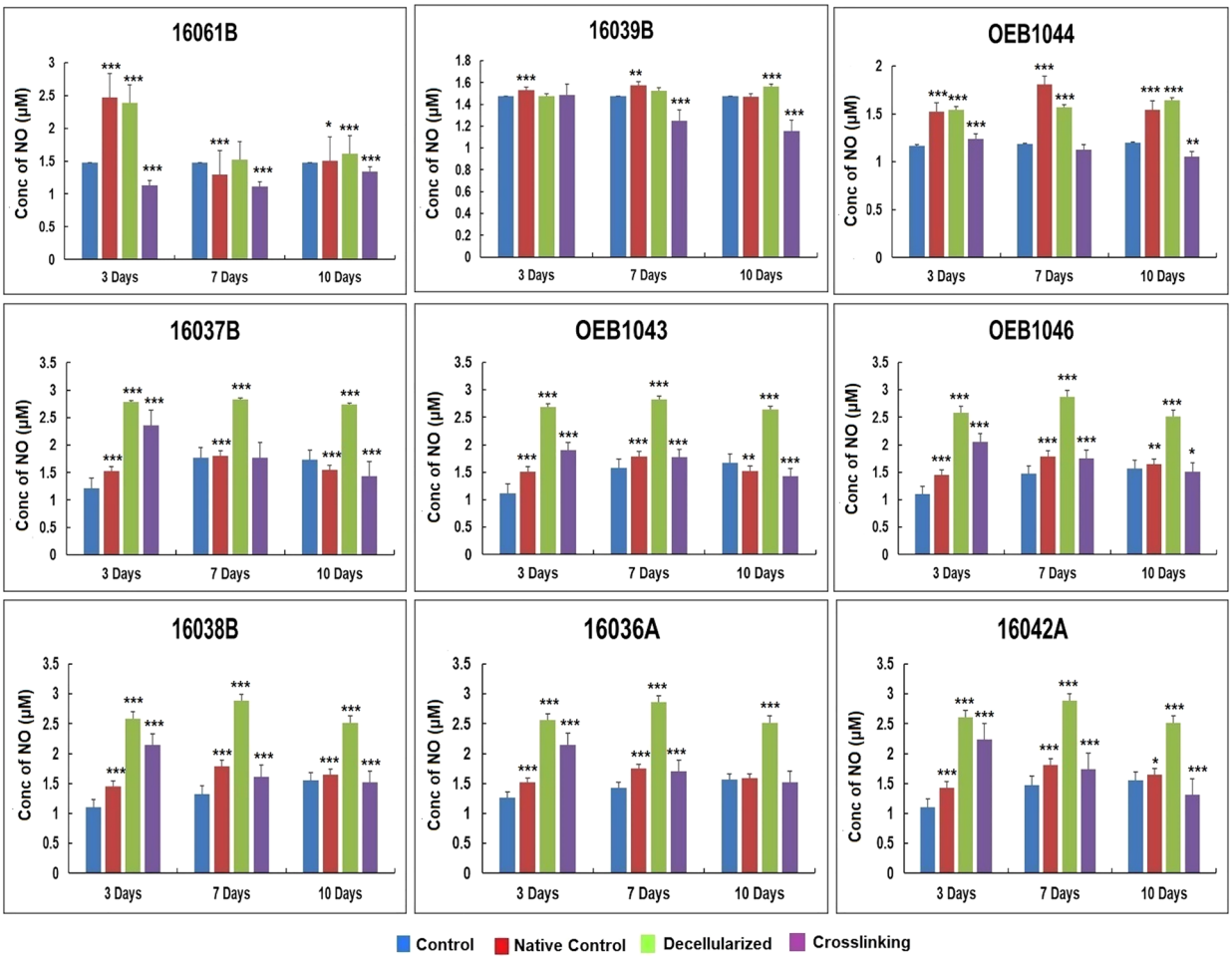

Figure 5: Release assay for nitric oxide in 16061B (A), 16039B (B), OEB1044 (C), 16037B (D), OEB1043 (E), OEB1046 (F), 16038B (G), 16036A (H), 16042A (I) nine patient sample at days 3, 7 and 10. GraphPad Prism 6 was used to perform one-way ANOVA. All data are presented as mean ± SD, statistical significance ($p < 0.05$). Each experiment was performed in triplicates and repeated twice.

and 16042A). It showed [6 ± 0.02-fold ($p < 0.05$)] lower expression than monocytes grown on the DC (12 ± 1.1, $p < 0.001$). MMP13 showed a [3.5 ± 0.02-fold ($p < 0.05$)] lower expression in cells grown on the CS-cross-linked surface than in those grown on the DC surface. IL6R1 expression in all CS-cross-linked corneal samples showed a similar trend and exhibited [1.5 ± 0.02-fold ($p < 0.05$)] lower expression of IL6R1 when compared with the other DC (Fig. 6).

Immune response analysis to identify cellular plasticity

Microarray analysis was performed to identify healthy monocytes' chemokine and cytokine release profiles from different NC, DC, and CS-cross-linked patient samples. Lipocalin-2 expression was the highest in the cross-linked patient sample. The remaining DC samples also showed a deficient level of Lipocalin-2 expression, which aligns with inflammatory conditions and is the predominant M1 subtype in cultured monocytes. MCP-1 is a key factor that attracts macrophages to the sites of inflammation. NC and DC corneas exhibited high MCP-1 and MCP-2 expression levels in all patient samples. Monocytes cultured from cross-linked patient samples showed lower expression levels [4 ± 0.02-fold ($p < 0.05$)]. MIF is a key regulator of the immune system that regulates inflammation and is highly upregulated in monocytes cultured from all DC patient samples, whereas all cross-linked samples showed minimal activity. One of the main chemoattractants and the pro-inflammatory chemokine MIP-1a/MIP-1b were found to be highly upregulated [6 ± 0.02-fold ($p < 0.05$)] in NC and DC samples compared to the cross-linked ones. Procalcitonin is a crucial pro-inflammatory response in the innate immune system that has been used as a biochemical marker of inflammation for several decades. NC and DC samples showed [a 2.5 ± 0.02-fold ($p < 0.05$)] increase in procalcitonin levels compared to cross-linked corneas. Thrombomodulin

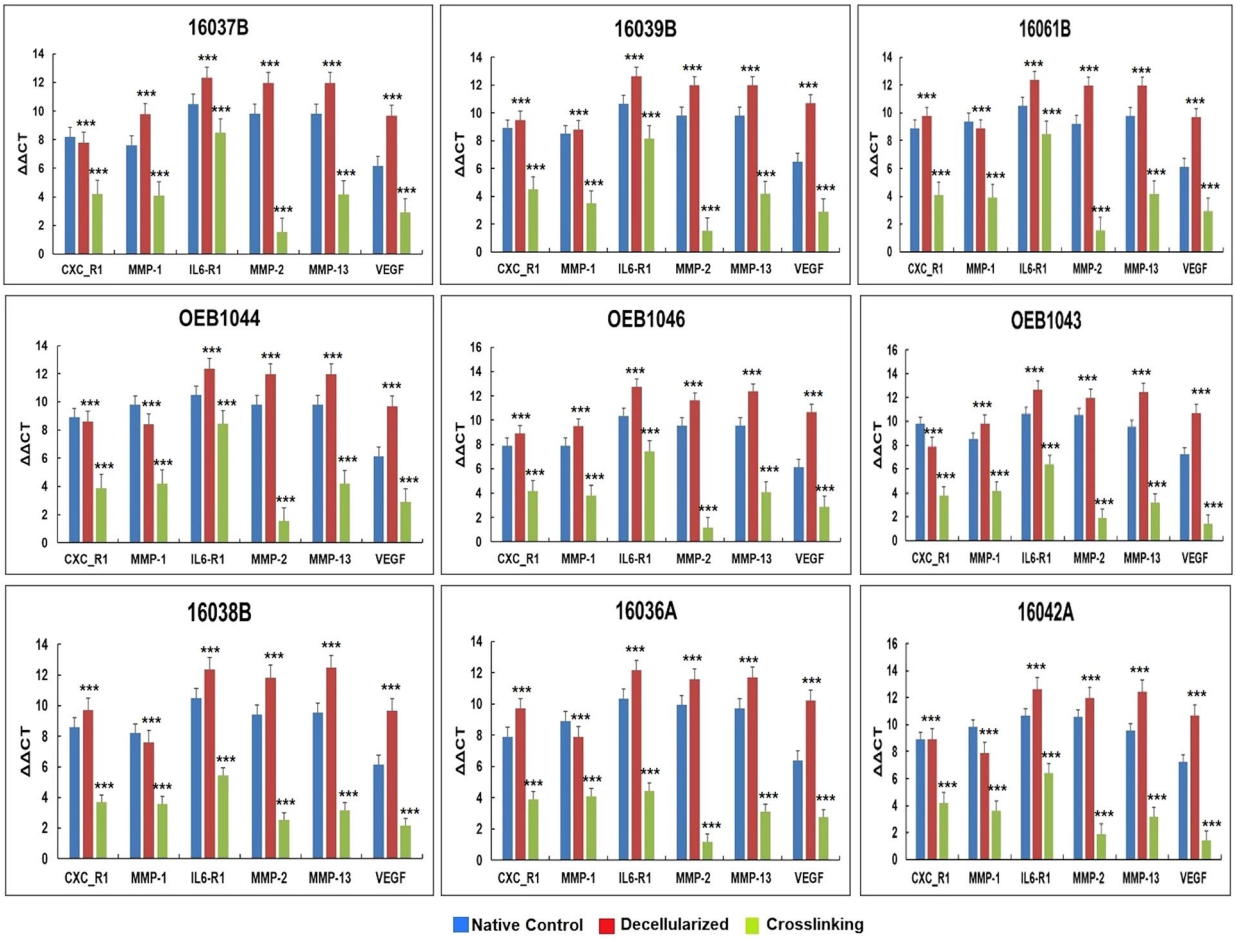

Figure 6: The gene expression profile for 16037B (A), 16039B (B), 16061B (C), OEB1044 (D), OEB1046 (E), OEB1043 (F), 16038B (G), 16036A (H), 16042A (I) nine cornea samples at day 10. List of gene screened CXCR1, IL6R1, MMP1, MMP2, MMP13, VEGF. GraphPad Prism 6 was used to perform one-way ANOVA. All data are presented as mean ± SD, statistical significance ($p < 0.05$). Each experiment was performed in triplicates and repeated twice.

is a transmembrane glycoprotein receptor that can suppress inflammatory responses and is highly expressed [4 ± 0.02-fold ($p < 0.05$)] in monocyte cultures on cross-linked corneal surfaces. DC and NC showed minimal thrombomodulin expression. Resistin and RAGE are both considered pro-inflammatory molecules of immune cells in the human body and were upregulated in DC and NC groups. VEGF expression was almost absent in the cross-linked groups of OEB1043, OEB1046, and 16036A patient samples, whereas 16042A and 16036A patient samples showed higher expression. TNF-α expression was [4 ± 0.02-fold ($p < 0.05$)] lower in all cross-linked patient samples than in DC samples (Fig. 7).

CD14 expression was highest in the DC group of all patient samples, with minimal expression [6.5 ± 0.02-fold ($p < 0.05$) lower] in the cross-linked patient group. High CD40 expression indicates macrophage recruitment and is evident in all DC patient samples. The cross-linked patient groups showed [2 ± 0.02-fold ($p < 0.05$)] lower expression than the DC. CRP was notably higher [2.5 ± 0.02-fold ($p < 0.05$)] in DC than in the cross-linked treatment groups. Fas and FAS L exhibited high levels of expression in the decellularized treatment group, indicating the inhibition of macrophage polarization toward the M2 phenotype. Pro-inflammatory cytokines were highly overexpressed (IL-1b, IL-6, IL-8, IL-12p70, and IL-18) in all DC compared with the cross-linked group. IL-1b and IL-18 expression were minimal in monocytes cultured in the cross-linked group. The levels of anti-inflammatory cytokines (IL-2, IL-2Ra, IL-4, IL-10, and IL-13) were elevated in all cross-linked samples (Fig. 8).

Bioinformatics analysis revealed that incubation with DC and NC monocytes increased pro-inflammatory cytokine levels (Lipocalin-2, MCP-1, MCP-2, MIP-1a/MIP-1b, Resistin, RAGE, IL-1b, IL-6, IL-8, IL-12p70, and IL-18). After incubation for 10 days, the increased pro-inflammatory cytokine levels exhibited an M1 phenotype. The levels of anti-inflammatory cytokines (IL-2, IL-2Ra, IL-4, IL-10, IL-13, and thrombomodulin) were elevated in all cross-linked patient samples [Fig. 9(A), (B)]. Through KEGG [Fig. 9(C)] analysis, we identified the top 20

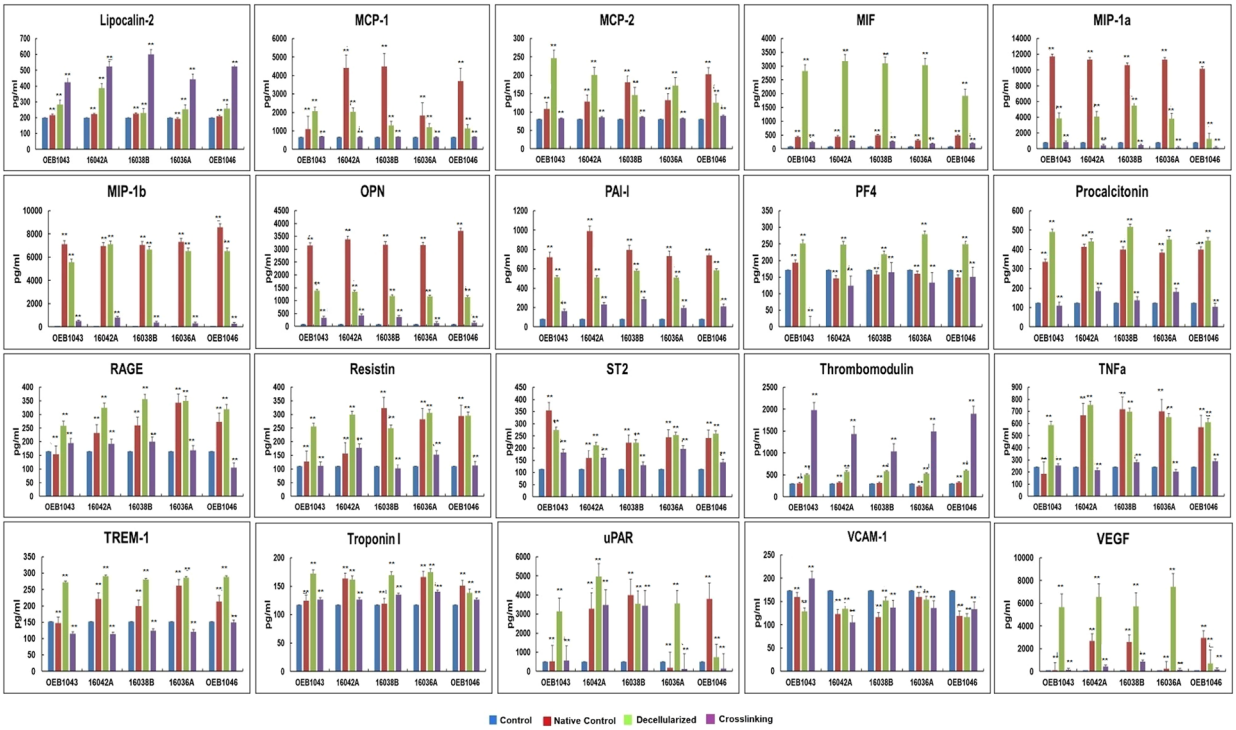

Figure 7: Human immune response array analysis of 20 (Lipocalin-2, MCP-1, MCP-2, MIF, MIP-1α, MIP-1β, OPN, Procalcitonin, Thrombomodulin, Resistin, RAGE, TNF, TREM-1, Troponin-1, VEGF, VCAM-1, ST-2, PAF4) selected cytokines (pg/mL) on five patient samples, at day 10. Each sample has been arrayed in quadruplicate. GraphPad Prism 6 was used to perform one-way ANOVA. All data are presented as mean ± SD, statistical significance ($p < 0.05$). Each experiment was performed in triplicates and repeated twice.

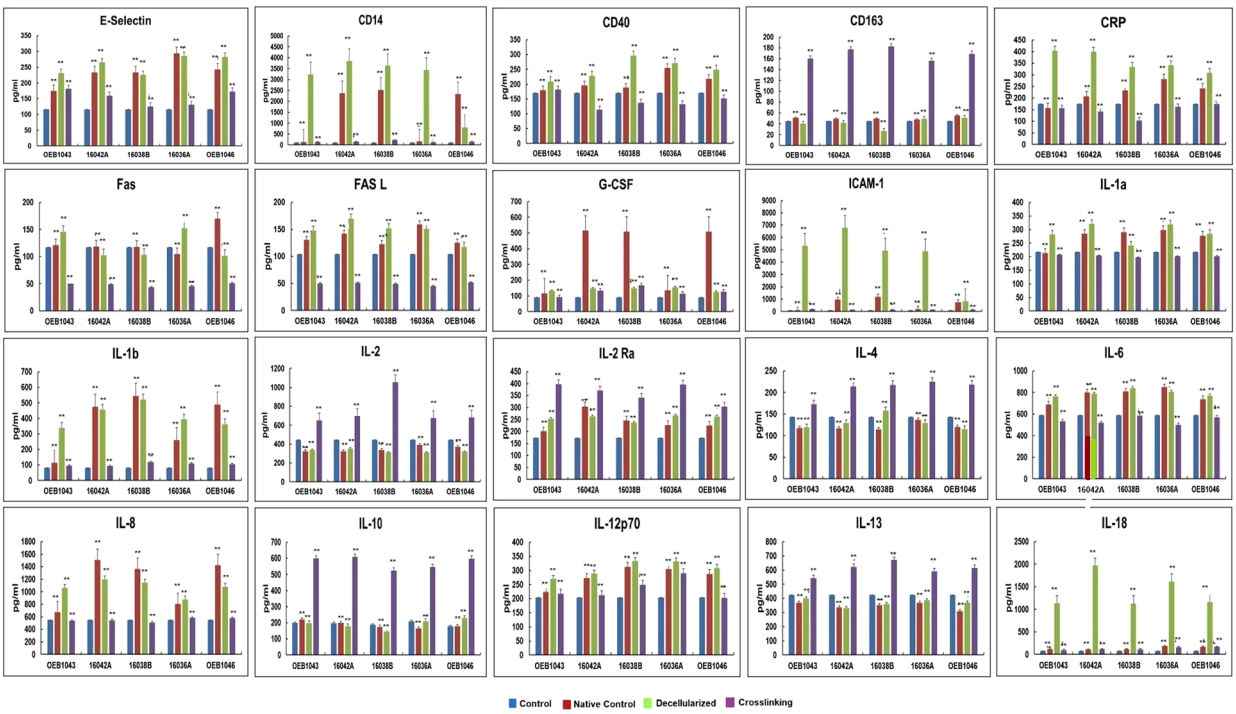

Figure 8: Human immune response array analysis of 20 (IL-1a, IL-1b, IL-2, IL-2Ra, IL-4, IL-6, IL-8, IL-10, IL-13, IL-18, IL-12p70, CD14, CD40, CD163, CRP, FAS, FASL, GCSF, E-selectin, ICAM-1) selected cytokines (pg/mL) on five patient samples. (OEB1043, 16042A, 16038B, 16036A, OEB1046) at day 10. Each sample has been arrayed in quadruplicate. GraphPad Prism 6 was used to perform one-way ANOVA. All data are presented as mean ± SD, statistical significance ($p < 0.05$). Each experiment was performed in triplicates and repeated twice.

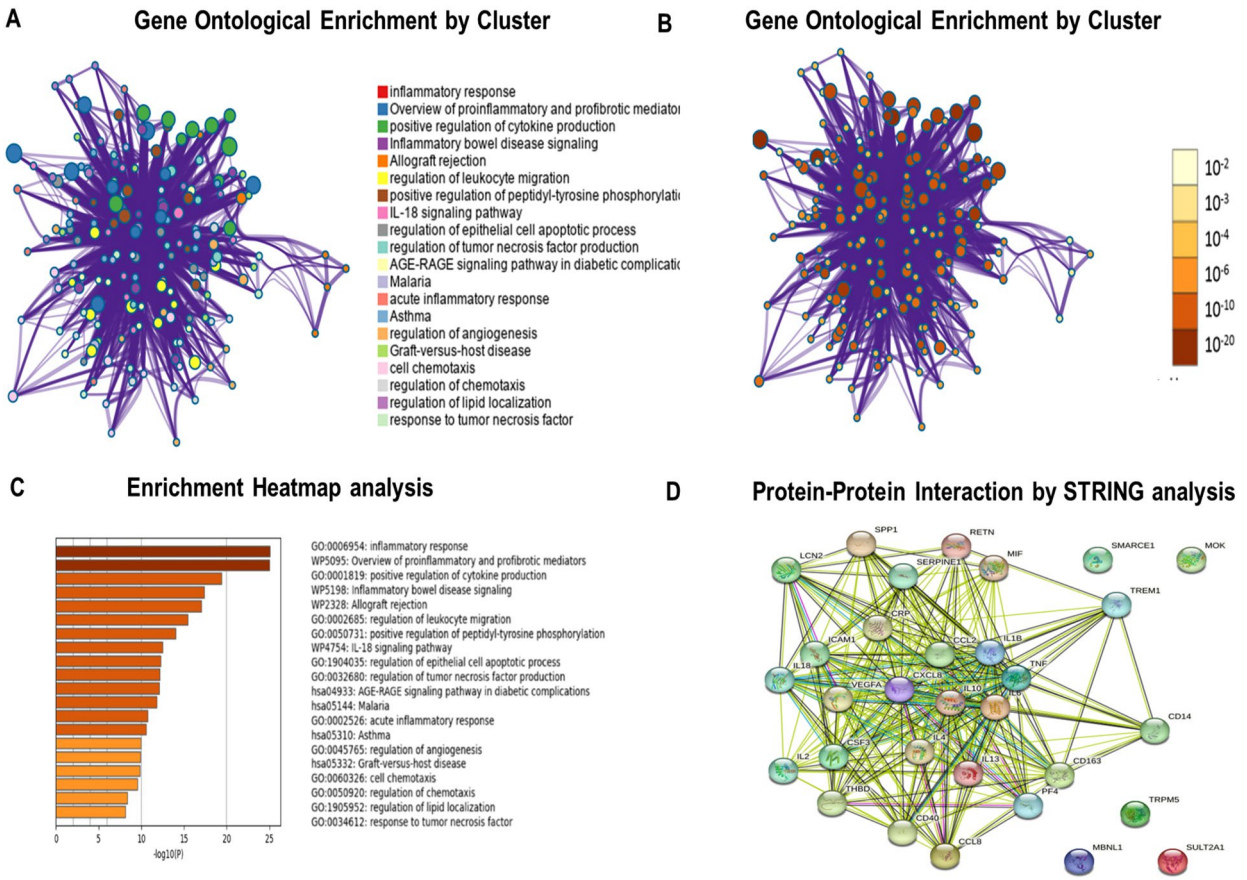

Figure 9: Gene Ontological enrichment by cluster, Gene Ontological enrichment by *p* value, Enrichment Heatmap analysis, and Protein–Protein Interaction by STRING analysis.

biological processes associated with these cytokines ($p < 0.05$), which were highly relevant for predicting the immunological profile. We constructed a PPI network string to identify the intermediate correlation between upregulated and downregulated cytokine release profiles. PPI network of NC and DC samples (16039B, OEB1043, 16036A, 16042A) reveals that MCP-1, MCP-2, MIP-1a/MIP-1b, IL-1b, IL-6, IL-8, IL-18, IL-2, IL-2Ra, IL-4, IL-10, IL-13, and thrombomodulin were the primary hub gene [Fig. 9(D)]. The percentage of anti-inflammatory cytokines (IL-2, IL-2Ra, IL-4, IL-10, IL-13, and thrombomodulin) increased by 32% of the total cytokines released after 10 days of incubation with the cross-linked patient sample.

Discussion

Despite numerous studies on reducing the host immune response after implantation, using macrophages to control and trigger tissue regeneration remains challenging in regenerative medicine. The cellular mechanism of corneal graft rejection is based solely on animal models [32–34]. Wolf et al. stimulated macrophages on allogeneic human corneal tissue with LPS and IFN to mimic the corneal graft rejection scenario. The immunogenic signature presented by the allogenic corneal tissue and specific identification of the macrophage subtype is inconclusive [35]. The present study studied detailed macrophage differentiation/plasticity using biochemical, genomic, and microarray assays in different experimental groups further to explore the role of resident and infiltrating macrophages and complement existing animal models. Before moving to human clinical trials, detailed surface and release marker analyses are needed using a well-established in vitro setup based on human cells. This will help identify the proper subtype to predict clinical outcomes more accurately.

In a previous study, we standardized the CS-mediated cross-linking of DC [16]. Based on the FTIR analysis, C=C stretching (1635 cm^{-1}) and D-NH_2 scissoring (1633 cm^{-1}) were visible in the NC and DC. These bands denote the changes in the corneal stromal collagen type 1 layer. In the cross-linked sample, the amide band shifted to a much lower wavenumber 1628 cm^{-1}. This observation indicates that oxidized CS interacts with C=O (collagen type 1) through COO^- and SO_3^- linkage [16]. During decellularization, changes in ECM ultrastructure were evident from the lamellar orientation and fibril density. CS cross-linking

helps maintain lamellar orientation and regular collagen diameter [36, 37].

After obtaining evidence of the successful cross-linking of CS by FTIR, we determined the differences in the three decellularized matrix surface topographies. The correlation between biophysics and macrophage material biology is a hot topic but is still in its infancy. Several studies have described the effects of surface roughness on cell spreading, protein absorption, adhesion, and plasticity [28, 38]. Controversy exists in the opinion given by different authors recently regarding the role of surface roughness in macrophage plasticity. Navarrete et al. found that activation of the M1 phenotype was induced by smooth titanium and the M2 phenotype by hydrophilic rough titanium [39]. Studies have reported that increased surface roughness can contribute to the release of pro-inflammatory cytokines through the M1 phenotype [39, 40]. Our study observed that the DC exhibited higher surface roughness than the NC. After decellularization, extensive collagen fibril orientation was observed due to the removal of cellular components, leading to increased surface roughness. Proteoglycans play versatile roles in maintaining lamellar assembly and collagen fibril orientation in the human cornea. CS cross-linking helps bridge the *N*-hydroxy succinimide (NHS) to the collagen and proteoglycan in the DC, which ultimately helps to stabilize the corneal ultrastructure with reduced surface roughness [26]. The AFM results support our FTIR findings and the hypothesis that CS-cross-linked corneas show lower surface roughness than DC. Our research revealed that the physicochemical properties of the DC could manipulate cellular plasticity and phenotyping of macrophages. This will help to identify advanced decellularized ECM with tunable immunomodulatory properties.

The effects of the surface roughness on the adhesion and diffusion of macrophages with different plasticities were explored using SEM in downstream experiments. Monocytes cultured on a DC showed round and pan-cake-like flattened morphology with no extracellular projections, similar to the findings of McWhorter et al. [41]. The cells were flattened and appeared to penetrate the matrix with visible degradation. Monocytes grown on CS-cross-linked surfaces exhibited an opposite pattern. Adhesion-activation morphology and elongated cells with extensive extracellular projections were observed in the cross-linked samples, indicating M2 plasticity. Our study provides crucial information that the physical properties of the ECM (architecture, mechanics, and surface topology) can change the immune cell phenotype [42, 43]. Decellularized ECM has the highest surface roughness, with the risk of exposure to a hidden antigenic motif of the collagen layer during the decellularization procedure [17]. Our study provides crucial information regarding the contribution of surface roughness to cellular plasticity. The CS-cross-linked patient sample with moderate surface roughness contributed to the elongated M2-like morphology of the patient sample. A better understanding of this biophysical environment will help to develop an immune-informed ECM with predictive immune compatibility.

We extended our study to identify the biochemical release patterns of monocytes (ROS and NO) cultured on NC, DC, and CS-cross-linked samples. Several studies have used multiple biomaterials to eliminate reactive oxygen species (ROS) after implantation [44–46]. However, a significant challenge remains to develop an effective and functionalized decellularized matrix that can sense ROS scavenging and direct M2 macrophage plasticity. CS has a long history of antioxidant potential with reduced liposome and high-density lipoprotein (HDL) oxidation [47, 48]. Similar patterns were observed in this study. Increased NO is a part of arginine metabolized to NO and citrulline, which can increase downstream ROS levels [49]. The CS-cross-linked patient group exhibited lower levels of ROS and NO than the decellularized group, which could reduce inflammation by ROS scavenging and promote the polarization of the M2 phenotype through the arginine pathway [50, 51].

We conducted this study to determine the gene expression and cytokine microarray profiles of 40 pro- and anti-inflammatory panels selected from all patient samples. Increased MMP1, 2 and 13 levels were observed in all decellularized patient samples, which can degrade the ECM and modulate cytokine and chemokine activities [52]. IL6R1-mediated induction of VEGF expression was observed in all decellularized patient samples. However, cross-linked corneal samples showed 10-fold lower VEGF and IL6R1 activity. Lipocalin-2 is a 25 kDa secreted protein, also known as gelatinase-associated lipocalin. Emerging evidence indicates that lipocalin-2 is highly overexpressed under anti-inflammatory conditions and can downregulate the expression of MCP-1 and TNF-α [53, 54]. A previous study suggested that lipocalin-2 is anti-inflammatory by controlling the NFκB-STAT3 loop and promoting M2 polarization [55]. Our results also indicated that the decellularized samples exhibited a 2-fold decrease in Lipocalin-2 expression, whereas the CS-cross-linked samples showed high levels of expression. MCP-1, MIF, and MIP-1a/MIP-1b levels were relatively high in all decellularized patient samples compared with those in the CS-cross-linked groups. It acts as a pleiotropic inflammatory mediator and chemoattractant and is responsible for immune cell recruitment, migration, and activation in inflammatory conditions [56–58]. Thrombomodulin is believed to suppress tissue inflammation via endocytosis and the protein C-dependent pathway [59]. Protein C activation activates a series of downstream pathways, such as reduced neutrophil infiltration and pro-inflammatory cytokine release by M1 phenotypes [60, 61]. Thrombomodulin also controls the dynamic M1/M2 switch through the IL-4R-c-Myc-pSTAT6-PPARγ axis, the main factor in M2 polarization. In our study, we observed a high level of thrombomodulin expression [4 ± 0.02-fold ($p < 0.05$)] in the CS-cross-linked

groups compared with that in the DC. This indicated that the M2 subtype was predominant in the CS-cross-linked samples. Resistin and RAGE are both pro-inflammatory and regulate diverse biological processes. Resistin is a selective adipokine that promotes the M1-like phenotype and has pro-inflammatory properties [62]. The receptor for advanced glycation end products (RAGE) is a member of the immunoglobulin superfamily, which tends to accumulate during inflammation and oxidative stress [63, 64]. Resistin and RAGE levels were upregulated in all decellularized patient samples. A similar pattern of high VEGF expression in all decellularized samples supports our previous findings regarding gene expression. The pro-inflammatory (IL-1b, IL-6, IL-8, IL-12p70, IL-18) and anti-inflammatory (IL-2, IL-2Ra, IL-4, IL-10, IL-13) cytokine groups showed a unique balance in our experimental findings. Monocytes grown on DC and NC samples exhibit high levels of pro-inflammatory interleukins.

GO and heat enrichment analyses revealed that DC and discarded NC showed high levels of an inflammatory response (pro-inflammatory mediators and acute immune response), allograft rejection, and positive regulation of IL-18 signaling. The cross-linked patient samples showed positive regulation of cytokine production, leukocyte migration, TNF production, angiogenesis, and chemotaxis.

Conclusions

Although several advancements have been made in decellularizing the human cornea over the past decade, its translational ability and predictive transplant immunology remain significant challenges. The present study established the potential use of decellularized and cross-linked discarded human corneas for penetrating anterior lamellar keratoplasty. This study revealed a potential difference in immunogenicity between decellularized and CS-cross-linked human corneas. Monocytes cultured on NC and DC surfaces exhibited a round, pan-cake-like M1 morphology, whereas CS-cross-linked samples showed extensive extracellular projections with filopodia, which denote M2 morphology. Hence, the CS-cross-linked decellularized sample polarizes monocytes into M2 subtypes. The biochemical release pattern of NO and ROS helped us to connect redox kinetics with cellular plasticity. Gene expression and human immune response array to identify the plasticity of healthy monocytes cultured on different corneal surfaces. Monocytes cultured on NC and DC samples showed high levels of pro-inflammatory cytokines, whereas the CS-cross-linked sample showed an anti-inflammatory response. Inflammation and macrophage response after transplantation are obvious processes in the intimal at 1–2 weeks. This study demonstrated that macrophages are directly correlated with graft rejection. Extensive identification of M1 and M2 macrophages on the corneal surface over 10 days will help predict the future of the transplantable decellularized matrix and its immunogenic profile. We found that monocytes cultured on CS-cross-linked DC changed their plasticity to the anti-inflammatory or M2 subtypes. This helps to predict the role of resident macrophages after implantation and their influence on in vivo reprogramming.

The use of culture-positive/serology-positive corneas is a future hurdle in developing fully biocompatible decellularized matrices. Stringent immunogenic checkpoints to evaluate the biocompatibility of CS-cross-linked decellularized matrix, preoperative antibiotic prophylaxis, and additional antifungal agents in preservation media may overcome this problem. Our comprehensive in vitro study will help identify the immunogenic profile of the decellularized cornea before transplantation and act as a gold standard alternative to currently available animal models.

Materials and methods

Materials

All materials were used as provided by the manufacturer unless mentioned otherwise. The RPMI-1640 medium (Cat. No. 1875093, Gibco), DMEM (Cat. No. 11965-092, Gibco), HEPES buffer (Cat. No. TCL021; HiMedia) and sodium bicarbonate (Cat. No. 11360-070, Gibco) and glutamine (Cat. No. TCL012; HiMedia) and penicillin–streptomycin–glutamine (PSG) (Cat. No. 10378016, Gibco), fetal bovine serum (FBS) (Cat. No. 10438-026, Gibco), and collagenase type-2 (Cat. No. 17101-015 Gibco), and phosphate-buffered saline (PBS) (Cat. No. SH30256.01; HyClone), antibiotic/antimycotic (AB/AM) solution (Cat. No. SV30079.01; HyClone), phorbol 12-myristate 13-acetate (PMA) (Cat. No. P8139; Sigma-Aldrich) and IL-4 (Cat. No. TC362; HiMedia) and IL-10 (Cat. No. TC424, HiMedia), and RNeasy Mini Kit (Cat. No. 74104, Qiagen), and a cDNA synthesis kit (Cat. No. K1621, Thermo Scientific), SYBR Green Master Mix (Cat. No. 204145, Qiagen), GAPDH, MMP1, MMP2, MMP13, CXCR1, IL6R1, VEGF (Supplementary Table 1), and the ROS assay kit (Cat. No. CCK071 EZ Assay, HiMedia) and nitric oxide (NO) (Cat. No. CCK061, EZ Assay, HiMedia). The Human Immune Response Array Kit (QAH-IMR-1-2; RayBiotech) was used.

Cornea Collection: The study was performed following the tenets of the declaration of Helsinki and started after the approval of the ethics committee, AIIMS

Two types of discarded human corneal remnants (residual tissue after transplantation) (RIM+ An anterior lamellar residual corneoscleral RIM) were observed. Discarded corneal samples that were unsuitable for further surgical procedures were used

in this study. The anterior lamella was obtained from the tissues used for endothelial keratoplasty. First, the donor cornea was processed for customized component surgery, the endothelial descemet complex was transplanted, and the anterior lamella was discarded, making it unsuitable for transplantation. The second type of tissue was obtained as residual corneal remnants after preparing the donor tissue for patch grafting. We used discarded surgical byproducts that were not useful for future clinical applications. The third type of processed specimen was culture-positive/serology-positive/poor endothelial status corneas that were unsuitable for transplantation and were set aside for biohazard disposal by the eye bank with no clinical applications. The details of all the samples are provided in the Supplementary Section (Supplementary Table 2). All the samples were collected in accordance with the ICH-GCP guidelines of the Ethics Committee of AIIMS, New Delhi (Ethical Approval—IEC-127/ 05.04.2019, RP-50.2019).

Decellularization and cross-linking with CS

The discarded human cornea was decellularized using a perfusion bioreactor (provided by Prof. Ivan Martin, Basel, Switzerland) according to the standardized protocol established in our laboratory [8]. Unidirectional constant flow (50 µL/min for 48 h) of Triton-X 100 (0.5% in PBS) through a peristaltic pump was perfused into corneal tissue. After decellularization, the tissue was rinsed with the PBS/antibiotic solution at a constant flow rate (10 µL/min for 48 h). 600 mg of CS was mixed with 616 mg of $NaIO_4$ in 10 mL deionized water (1 h, 40 °C, continuous stirring, dark) to obtain oxidized CS. Oxidized CS was purified using Sephadex G-25 size-exclusion chromatography. The decellularized cornea was pretreated with sodium acetate solution (10% w/v, 1 h) before incubation with oxidized CS.

Glycosaminoglycan (GAG) quantification

The dimethyl methylene blue (DMMB) assay was used to determine the residual GAG content in the chemically processed decellularized human corneal tissues. The sections were immersed in 50 mL of proteinase K (SRL, India) at 56 °C overnight for enzymatic treatment. Tissue fragments that had been digested were examined for GAG concentration. Dry tissue weight was used to standardize all measured quantities. The microplate reader was used to take the spectrophotometric values at 525 nm (Thermofisher, USA) (Supplementary Table 7).

DNA quantification

Human native and decellularized corneal DNA was extracted using a DNA extraction kit (Agilent Technologies, Germany) guideline. The spectrophotometer (Thermofisher Scientific, USA) was used for the quantification (Supplementary Table 7).

Cell culture

THP-1 cells were collected from the National Center for Cell Science, Pune, and are hereafter referred to as "monocytes." Monocytes were cultured in RPMI-1640 medium supplemented with 1% PSG and 10% heat-inactivated FBS. Healthy monocytes were cultured on native, decellularized, and cross-linked corneal surfaces for 10 days. The constructs were then incubated at 37 °C in a 5% CO_2 atmosphere [65].

Attenuated total reflectance-Fourier transform infrared spectroscopy (ATR-FTIR)

An Alpha-P spectroscope (Bruker, USA) was used to obtain ATR-FTIR spectra of the freeze-dried native, decellularized, and CS-cross-linked decellularized corneal samples. 240 infrared spectrum scans were taken in transmittance mode in the spectral region of 400–4000 cm^{-1} with a spectral resolution of 4 cm^{-1} for each sample. Deconvolution in the range of 900–1800 cm^{-1} was done and the peaks in the spectral area were obtained using Origin 8.5.

Determination of topographical features using atomic force microscopy (AFM)

Topographical changes on the surfaces of different corneal matrices were determined using AFM. The surface morphology was determined in the contact mode using the Asylum Research MFP3D-SA. Micrographs were captured using a Tap300AI cantilever with a spring constant of 40 N/m and a resonance frequency of 300 kHz at a scanning rate of 0.5 at different scanning areas. Imaging was performed at various scales to identify the required properties.

Scanning electron microscopy

All three samples (native, decellularized, and cross-linked) were fixed in 4.2% paraformaldehyde for 10 min in the dark. The samples were then washed with PBS, dehydrated with alcohol, and graded. Gold sputter coating (15–20 nm) was performed using an EMITECH K550X (25 mA for 240 s) before final processing. All the samples were imaged using a JEOL 5610 LV instrument at an accelerating voltage of 5 kV. The samples were imaged at two different magnifications, × 2000 and × 5000, with scale bars of 10–2 µm.

Antioxidant and nitric oxide (NO) estimation

Estimation of released reactive oxygen species (ROS)

Antioxidant activity was estimated according to the manufacturer's instructions using the EZ Assay™ ROS Activity Estimation Kit (HiMedia). According to this principle, the ferric ion–chromogen complex is reduced to colored ferrous ions at low pH. The media (3, 7, and 10 days) of THP-1 monocytes cultured with different groups of human corneas were compared to those of untreated cells. FRAP values were obtained by comparing the absorbance change at 593 nm in the test reaction mixtures containing ferrous ions at known concentrations.

Estimation of NO release

NO was estimated according to the manufacturer's instructions using the EZ Assay™ NO Estimation Kit. The principles of the assay are based on the reduction of nitrate to nitrite by reducing agents. Total nitrite was converted to a blue-colored azo compound using the Griess reagent for spectrophotometric detection. The media (3, 7, and 10 days) of THP-1 monocytes cultured with different groups of human corneas were compared with those of untreated cells. The absorbance was recorded at 560 nm. This assay was performed separately to identify free nitrate and nitrite ions.

Gene expression analysis

After 10 days, THP-1 monocytes were treated with 1 mL of cell lysis buffer in tissue culture plates. The cell lysates were collected on days 1, 3, and 7. Total RNA was extracted using the RNeasy Mini Kit according to the manufacturer's protocol. The total extracted RNA was reverse-transcribed into cDNA using a first-strand cDNA synthesis kit, and real-time PCR was conducted using SYBR Green Master Mix and a Rotor gene Q thermocycler. Rotor gene Q software was used for the analysis, and the relative fold change in expression levels was calculated using the $2^{-(\Delta\Delta c(t))}$ method with GAPDH as the housekeeping gene. THP-1 monocytes on day 1 were used as comparators or controls to calculate the delta–delta C_t relative fold change. The expression levels of MMP1, MMP2, MMP13, CXCR1, IL6R1, and VEGF were evaluated.

Immune response array analysis

The supernatant was collected from the negative control and all patient groups after 10 days of THP-1 cell culture. The experiment was performed according to the manufacturer's instructions for the human immune response array Q1 [QAH-IMR-1-2]. Following cytokine and protein CD14, CD163, CD40 (TNFRSF5), CRP (C-Reactive Protein), E-Selectin, Fas (TNFRSF6/Apo-1), Fas Ligand (TNFSF6), GCSF, ICAM-1 (CD54), IL-1 alpha (IL-1 F1), IL-1 beta (IL-1F2), IL-1 R4 (ST-2), IL-10, IL-12 p70, IL-13, IL-18, IL-2, IL-2 Ralpha, IL-4, IL-6, IL-8 (CXCL8), Lipocalin-2 (NGAL), MCP-1(CCL2), MCP-2 (CCL8), MIF, MIP-1 alpha (CCL3), MIP-1beta (CCL4), Osteopontin (SPP1), PAI-1, Platelet Factor 4(CXCL4), Procalcitonin, RAGE, Resistin, Thrombomodulin, TNF alpha, TREM-1, Troponin I, uPAR, VCAM-1 (CD106), VEGF-A was examined to identify differential release patterns of THP-1 cells on the corneal surface. All cytokines were arrayed in quadruplicates. Fluorescence was measured in the Cy3 channel at 532 nm using GenePix4000B, and the gal file was extracted using GenePix Pro 7.2.22 microarray analysis software.

GO, KEGG pathway enrichment analysis, and protein–protein interactions

Gene ontological analysis (http://www.geneontology.org) and Kyoto Encyclopedia of Genes and Genomes (KEGG) pathway enrichment analysis were performed using Metascape (https://metascape.org) to identify alterations in expression through microarray analysis. A p value of < 0.05 was considered significant for data analysis and visualization of the correlated gene in the heatmap. We used Genemania (http://genemania.org) to build a protein–protein network of different cytokines to predict the network pharmacology. We identified the selected genes with a high node degree using STRING (http://string-db.org).

Statistical analysis

GraphPad Prism 6 was used to perform one-way ANOVA. All data are presented as mean ± SD. Statistical significance was established at ($p < 0.05$). Each experiment was performed in triplicates and repeated twice.

Acknowledgments

JC is grateful to the Department of Science and Technology (DST), India, for the Inspire Fellowship (SRF) No. IF160365. We acknowledge the Advanced Equipment Facility (AEF), THSTI, Faridabad, India, for providing the microarray scanning (GenePix 4000B, Molecular Devices) Facility.

Funding

None.

Data availability

The datasets used and analyzed during the current study are available from the corresponding author upon reasonable request.

Declarations

Conflict of interest No conflict of interest exists for any author.

Ethical approval

IEC-127/ 05.04.2019, RP-50.2019.

Supplementary Information

The online version contains supplementary material available at https://doi.org/10.1557/s43578-023-01182-8.

References

1. S.K. Chauhan, T.H. Dohlman, R. Dana, Corneal lymphatics: role in ocular inflammation as inducer and responder of adaptive immunity. J. Clin. Cell. Immunol. **5**(05), 1000256 (2014)
2. S. Nair, A.M.J. Buiting, R.J.D. Rouse, N. Van Rooijen, L. Huang, B.T. Rouse, Role of macrophages and dendritic cells in primary cytotoxic T lymphocyte responses. Int. Immunol. **7**(4), 679 (1995)
3. E.J. Holland, T.W. Olsen, C.C. Chan, L. Bergstrom, A.G. Palestine, R.B. Nussenblatt, Kinetics of corneal transplant rejection in the rat penetrating keratoplasty model. Cornea **13**(4), 317 (1994)
4. K. Hadrian, S. Willenborg, F. Bock, C. Cursiefen, S.A. Eming, D. Hos, Macrophage-mediated tissue vascularization: similarities and differences between cornea and skin. Front. Immunol. **12**, 1114 (2021)
5. Z. Wang, A.L. Koenig, K.J. Lavine, R.S. Apte, Macrophage plasticity and function in the eye and heart. Trends Immunol. **40**(9), 825 (2019)
6. M. Eslani, I. Putra, X. Shen, J. Hamouie, A. Tadepalli, K.N. Anwar, J.A. Kink, S. Ghassemi, G. Agnihotri, S. Reshetylo, A. Mashaghi, R. Dana, P. Hematti, A.R. Djalilian, Cornea-derived mesenchymal stromal cells therapeutically modulate macrophage immunophenotype and angiogenic function. Stem Cells (Dayt. Ohio) **36**(5), 775 (2018)
7. S. Nara, S. Chameettachal, S. Midha, H. Singh, R. Tandon, S. Mohanty, S. Ghosh, Strategies for faster detachment of corneal cell sheet using micropatterned thermoresponsive matrices. J. Mater. Chem. B **3**(20), 4155 (2015)
8. S. Nara, S. Chameettachal, S. Midha, S. Murab, S. Ghosh, Preservation of biomacromolecular composition and ultrastructure of a decellularized cornea using a perfusion bioreactor. RSC Adv. **6**(3), 2225 (2015)
9. Y. Zhang, H. Luo, Z. Zhang, Y. Lu, X. Huang, L. Yang, J. Xu, W. Yang, X. Fan, B. Du, P. Gao, G. Hu, Y. Jin, A nerve graft constructed with xenogeneic acellular nerve matrix and autologous adipose-derived mesenchymal stem cells. Biomaterials **31**(20), 5312 (2010)
10. S.R. Meyer, B. Chiu, T.A. Churchill, L. Zhu, J.R.T. Lakey, D.B. Ross, Comparison of aortic valve allograft decellularization techniques in the rat. J. Biomed. Mater. Res. A **79**(2), 254 (2006)
11. I. Prasertsung, S. Kanokpanont, T. Bunaprasert, V. Thanakit, S. Damrongsakkul, Development of acellular dermis from porcine skin using periodic pressurized technique. J. Biomed. Mater. Res. B **85**(1), 210 (2008)
12. B.S. Kim, H. Kim, G. Gao, J. Jang, D.W. Cho, Decellularized extracellular matrix: a step towards the next generation source for Bioink manufacturing. Biofabrication **9**(3), 034104 (2017)
13. J. Liao, L. Yang, J. Grashow, M.S. Sacks, The relation between collagen fibril kinematics and mechanical properties in the mitral valve anterior leaflet. J. Biomech. Eng. **129**(1), 78 (2007)
14. Y. Yamada, S. Nakamura, K. Ito, T. Sugito, R. Yoshimi, T. Nagasaka, M. Ueda, A feasibility of useful cell-based therapy by bone regeneration with deciduous tooth stem cells, dental pulp stem cells, or bone-marrow-derived mesenchymal stem cells for clinical study using tissue engineering technology. Tissue Eng. A **16**(6), 1891 (2010)
15. S. Murab, S. Ghosh, Impact of osmoregulatory agents on the recovery of collagen conformation in decellularized corneas. Biomed. Mater. (Bristol Engl.) **11**(6), 065005 (2016)
16. J. Chakraborty, S. Roy, S. Murab, R. Ravani, K. Kaur, S. Devi, D. Singh, S. Sharma, S. Mohanty, A.K. Dinda, R. Tandon, S. Ghosh, Modulation of macrophage phenotype, maturation, and graft integration through chondroitin sulfate cross-linking to decellularized cornea. ACS Biomater. Sci. Eng. **5**(1), 165 (2019)
17. J. Chakraborty, S. Roy, S. Ghosh, Regulation of decellularized matrix mediated immune response. Biomater. Sci. **8**(5), 1194 (2020)
18. N. Polisetti, A. Schmid, U. Schlötzer-Schrehardt, P. Maier, S.J. Lang, T. Steinberg, G. Schlunck, T. Reinhard, A decellularized human corneal scaffold for anterior corneal surface reconstruction. Sci. Rep. **11**(1), 1 (2021)
19. K. Chakrabarty, R. Shetty, A. Ghosh, Corneal cell therapy: with iPSCs, it is no more a far-sight. Stem Cell Res. Ther. **9**(1), 1 (2018)
20. J. Liu, Y. Xue, D. Dong, C. Xiao, C. Lin, H. Wang, F. Song, T. Fu, Z. Wang, J. Chen, H. Pan, Y. Li, D. Cai, Z. Li, CCR2– and CCR2+ corneal macrophages exhibit distinct characteristics and balance inflammatory responses after epithelial abrasion. Mucosal Immunol. **10**(5), 1145 (2017)
21. Y. Xue, J. He, C. Xiao, Y. Guo, T. Fu, J. Liu, C. Lin, M. Wu, Y. Yang, D. Dong, H. Pan, C. Xia, L. Ren, Z. Li, The mouse autonomic nervous system modulates inflammation and epithelial

renewal after corneal abrasion through the activation of distinct local macrophages. Mucosal Immunol. **11**(5), 1496 (2018)

22. J. Liu, M. Wu, J. He, C. Xiao, Y. Xue, T. Fu, C. Lin, D. Dong, Z. Li, Antibiotic-induced dysbiosis of gut microbiota impairs corneal nerve regeneration by affecting CCR2-negative macrophage distribution. Am. J. Pathol. **188**(12), 2786 (2018)
23. M. Wu, J. Liu, F. Li, S. Huang, J. He, Y. Xue, T. Fu, S. Feng, Z. Li, Antibiotic-induced dysbiosis of gut microbiota impairs corneal development in postnatal mice by affecting CCR2 negative macrophage distribution. Mucosal Immunol. **13**(1), 47 (2019)
24. S. Gordon, A. Plüddemann, Tissue macrophages: heterogeneity and functions. BMC Biol. **15**(1), 1 (2017)
25. J.M.G. Reyes, S. Herretes, A. Pirouzmanesh, D.-A. Wang, J.H. Elisseeff, A. Jun, P.J. McDonnell, R.S. Chuck, A. Behrens, A modified chondroitin sulfate aldehyde adhesive for sealing corneal incisions. Investig. Ophthalmol. Vis. Sci. **46**(4), 1247 (2005)
26. X. Wang, S. Majumdar, G. Ma, J. Sohn, S.C. Yiu, W. Stark, A. Al-Qarni, D.P. Edward, J.H. Elisseeff, Chondroitin sulfate-based biocompatible crosslinker restores corneal mechanics and collagen alignment. Investig. Ophthalmol. Vis. Sci. **58**(10), 3887 (2017)
27. Y. Henrotin, M. Mathy, C. Sanchez, C. Lambert, Chondroitin sulfate in the treatment of osteoarthritis: from in vitro studies to clinical recommendations. Ther. Adv. Musculoskelet. Dis. **2**(6), 335 (2010)
28. J. Solon, I. Levental, K. Sengupta, P.C. Georges, P.A. Janmey, Fibroblast adaptation and stiffness matching to soft elastic substrates. Biophys. J. **93**(12), 4453 (2007)
29. S. Jung, B. Pant, M. Climans, G. Curtis Shaw, E.-J. Lee, N. Kim, M. Park, Transformation of electrospun keratin/PVA nanofiber membranes into multilayered 3D scaffolds: physiochemical studies and corneal implant applications. Int. J. Pharm. **610**, 121228 (2021)
30. H. Bakhshandeh, M. Soleimani, S.S. Hosseini, H. Hashemi, I. Shabani, A. Shafiee, A.H.B. Nejad, M. Erfan, R. Dinarvand, F. Atyabi, Poly (epsilon-caprolactone) nanofibrous ring surrounding a polyvinyl alcohol hydrogel for the development of a biocompatible two-part artificial cornea. Int. J. Nanomed. **6**, 1509 (2011)
31. M. Bhattacharjee, S. Chawla, S. Chameettachal, S. Murab, N.S. Bhavesh, S. Ghosh, Role of chondroitin sulphate tethered silk scaffold in cartilaginous disc tissue regeneration. Biomed. Mater. (Bristol Engl.) **11**(2), 025014 (2016)
32. L. Kuffová, L. Lumsden, V. Veselá, J.A. Taylor, M. Filipec, V. Holán, A.D. Dick, J.V. Forrester, Kinetics of leukocyte and myeloid cell traffic in the murine corneal allograft response. Transplantation **72**(7), 1292 (2001)
33. T.P.A.M. Slegers, L. Broersma, N. Van Rooijen, J.M.M. Hooymans, G. Van Rij, R. Van Der Gaag, Macrophages play a role in the early phase of corneal allograft rejection in rats. Transplantation **77**(11), 1641 (2004)
34. G. Van der Veen, L. Broersma, C.D. Dijkstra, N. Van Rooijen, G. Van Rij, R. Van der Gaag, Invest. Ophthalmol. Vis. Sci. **35**(9), 3505 (1994)
35. J. Wolf, X. Zhuang, A. Hildebrand, S. Boneva, M. Schwämmle, P. Kammrath Betancor, J. Fan, D. Böhringer, P. Maier, C. Lange, T. Reinhard, G. Schlunck, T. Lapp, Corneal tissue induces transcription of metallothioneins in monocyte-derived human macrophages. Mol. Immunol. **128**(November), 188 (2020)
36. N.E. Vrana, N. Builles, V. Justin, J. Bednarz, G. Pellegrini, B. Ferrari, O. Damour, D.J.S. Hulmes, V. Hasirci, Development of a reconstructed cornea from collagen–chondroitin sulfate foams and human cell cultures. Investig. Ophthalmol. Vis. Sci. **49**(12), 5325 (2008)
37. D.A. Wang, S. Varghese, B. Sharma, I. Strehin, S. Fermanian, J. Gorham, D.H. Fairbrother, B. Cascio, J.H. Elisseeff, Multifunctional chondroitin sulphate for cartilage tissue-biomaterial integration. Nat. Mater. **6**(5), 385 (2007)
38. C. Rianna, M. Radmacher, Influence of microenvironment topography and stiffness on the mechanics and motility of normal and cancer renal cells. Nanoscale **9**(31), 11222 (2017)
39. K.M. Hotchkiss, G.B. Reddy, S.L. Hyzy, Z. Schwartz, B.D. Boyan, R. Olivares-Navarrete, Titanium surface characteristics, including topography and wettability, alter macrophage activation. Acta biomater. **31**, 425 (2016)
40. P.K. Viji Babu, C. Rianna, U. Mirastschijski, M. Radmacher, Nano-mechanical mapping of interdependent cell and ECM mechanics by AFM force spectroscopy. Sci. Rep. **9**(1), 1 (2019)
41. F.Y. McWhorter, T. Wang, P. Nguyen, T. Chung, W.F. Liu, Modulation of macrophage phenotype by cell shape. Proc. Natl. Acad. Sci. U.S.A. **110**(43), 17253 (2013)
42. C.Q. Lin, M.J. Bissell, Multi-faceted regulation of cell differentiation by extracellular matrix. FASEB J. **7**(9), 737 (1993)
43. A. Sica, A. Mantovani, Macrophage plasticity and polarization: in vivo veritas. J. Clin. Investig. **122**(3), 787 (2012)
44. Z. Liu, H. Wang, Y. Wang, Q. Lin, A. Yao, F. Cao, D. Li, J. Zhou, C. Duan, Z. Du, Y. Wang, C. Wang, The influence of chitosan hydrogel on stem cell engraftment, survival and homing in the ischemic myocardial microenvironment. Biomaterials **33**(11), 3093 (2012)
45. G. Choe, S.W. Kim, J. Park, J. Park, S. Kim, Y.S. Kim, Y. Ahn, D.W. Jung, D.R. Williams, J.Y. Lee, Anti-oxidant activity reinforced reduced graphene oxide/alginate microgels: mesenchymal stem cell encapsulation and regeneration of infarcted hearts. Biomaterials **225**, 119513 (2019)
46. T. Hao, J. Li, F. Yao, D. Dong, Y. Wang, B. Yang, C. Wang, Injectable fullerenol/alginate hydrogel for suppression of oxidative stress damage in brown adipose-derived stem cells and cardiac repair. ACS Nano **11**(6), 5474 (2017)
47. G. Campo, A. Avenoso, S. Campo, A. Ferlazzo, A. Calatroni, Chondroitin sulphate: antioxidant properties and beneficial effects. Mini Rev. Med. Chem. **6**(12), 1311 (2006)

48. Y.L. Jin, H.L. Sang, J.K. Hee, J.M. Ha, S.H. Lee, J.H. Lee, J.H. Bae, The preventive inhibition of chondroitin sulfate against the CCI4-induced oxidative stress of subcellular level. Arch. Pharmacal Res. **27**(3), 340 (2004)
49. E.M. Palmieri, M. Gonzalez-Cotto, W.A. Baseler, L.C. Davies, B. Ghesquière, N. Maio, C.M. Rice, T.A. Rouault, T. Cassel, R.M. Higashi, A.N. Lane, T.W.M. Fan, D.A. Wink, D.W. McVicar, Nitric oxide orchestrates metabolic rewiring in M1 macrophages by targeting aconitase 2 and pyruvate dehydrogenase. Nat. Commun. **11**(1), 1 (2020)
50. H.Y. Tan, N. Wang, S. Li, M. Hong, X. Wang, Y. Feng, The reactive oxygen species in macrophage polarization: reflecting its dual role in progression and treatment of human diseases. Oxid. Med. Cell. Longev. **2016**, 2795090 (2016)
51. J. Zhou, W. Liu, X. Zhao, Y. Xian, W. Wu, X. Zhang, N. Zhao, F.J. Xu, C. Wang, Natural melanin/alginate hydrogels achieve cardiac repair through ROS scavenging and macrophage polarization. Adv. Sci. **8**(20), 2100505 (2021)
52. P.T.G. Elkington, C.M. O'Kane, J.S. Friedland, The paradox of matrix metalloproteinases in infectious disease. Clin. Exp. Immunol. **142**(1), 12 (2005)
53. J.M. Warszawska, R. Gawish, O. Sharif, S. Sigel, B. Doninger, K. Lakovits, I. Mesteri, M. Nairz, L. Boon, A. Spiel, V. Fuhrmann, B. Strobl, M. Müller, P. Schenk, G. Weiss, S. Knapp, Lipocalin 2 deactivates macrophages and worsens pneumococcal pneumonia outcomes. J. Clin. Investig. **123**(8), 3363 (2013)
54. Y. Zhang, R. Foncea, J.A. Deis, H. Guo, D.A. Bernlohr, X. Chen, Lipocalin 2 expression and secretion is highly regulated by metabolic stress, cytokines, and nutrients in adipocytes. PLoS ONE **9**(5), e96997 (2014)
55. H. Guo, D. Jin, X. Chen, Lipocalin 2 is a regulator of macrophage polarization and NF-κB/STAT3 pathway activation. Mol. Endocrinol. (Baltim. Md.) **28**(10), 1616 (2014)
56. G. Grieb, M. Merk, J. Bernhagen, R. Bucala, Macrophage migration inhibitory factor (MIF): a promising biomarker. Drug News Perspect. **23**(4), 257 (2010)
57. I. Bhavsar, C.S. Miller, M. Al-Sabbagh, Macrophage inflammatory protein-1 alpha (MIP-1 alpha)/CCL3: as a biomarker. Gen. Methods Biomark. Res. Appl. **1–2**, 223 (2015)
58. L.B. Moore, A.J. Sawyer, A. Charokopos, E.A. Skokos, T.R. Kyriakides, Loss of monocyte chemoattractant protein-1 alters macrophage polarization and reduces NFκB activation in the foreign body response. Acta biomater. **11**(1), 37 (2015)
59. I. Maruyama, P.W. Majerus, The turnover of thrombin–thrombomodulin complex in cultured human umbilical vein endothelial cells and A549 lung cancer cells. Endocytosis and degradation of thrombin. J. Biol. Chem. **260**(29), 15432 (1985)
60. M. Van De Wouwer, D. Collen, E.M. Conway, Thrombomodulin-protein C-EPCR system: integrated to regulate coagulation and inflammation. Arterioscler. Thromb. Vasc. Biol. **24**(8), 1374 (2004)
61. P.P. Sarangi, H.W. Lee, M. Kim, Activated protein C action in inflammation. Br. J. Haematol. **148**(6), 817 (2010)
62. M.C. Zuniga, G. Raghuraman, E. Hitchner, C. Weyand, W. Robinson, W. Zhou, PKC-epsilon and TLR4 synergistically regulate resistin-mediated inflammation in human macrophages. Atherosclerosis **259**, 51 (2017)
63. R. López-Díez, A. Shekhtman, R. Ramasamy, A.M. Schmidt, Cellular mechanisms and consequences of glycation in atherosclerosis and obesity. Biochim. Biophys. Acta Mol. Basis Dis. **1862**(12), 2244 (2016)
64. A. Shekhtman, R. Ramasamy, A.M. Schmidt, Glycation and the RAGE axis: targeting signal transduction through DIAPH1. Expert Rev. Proteomics **14**(2), 147 (2017)
65. S. Roy, A. Sharma, S. Ghosh, Macrophage polarization profiling on native and regenerated silk biomaterials. ACS Biomater. Sci. Eng. **8**(2), 659 (2022)